Automatic Left Ventricle Segmentation Using Iterative Thresholding and an Active Contour Model With Adaptation on Short-Axis Cardiac MRI

Hae-Yeoun Lee, Noel C. F. Codella, Matthew D. Cham, Jonathan W. Weinsaft, and Yi Wang*

Abstract—An automatic left ventricle (LV) segmentation algorithm is presented for quantification of cardiac output and myocardial mass in clinical practice. The LV endocardium is first segmented using region growth with iterative thresholding by detecting the effusion into the surrounding myocardium and tissues. Then the epicardium is extracted using the active contour model guided by the endocardial border and the myocardial signal information estimated by iterative thresholding. This iterative thresholding and active contour model with adaptation (ITHACA) algorithm was compared to manual tracing used in clinical practice and the commercial MASS Analysis software (General Electric) in 38 patients, with Institutional Review Board (IRB) approval. The ITHACA algorithm provided substantial improvement over the MASS software in defining myocardial borders. The ITHACA algorithm agreed well with manual tracing with a mean difference of blood volume and myocardial mass being 2.9 ± 6.2 mL (mean $\pm$ standard deviation) and -0.9 ± 16.5 g, respectively. The difference was smaller than the difference between manual tracing and the MASS software (approximately -20.0 ± 6.9 mL and -1.0 ± 20.2 g, respectively). These experimental results support that the proposed ITHACA segmentation is accurate and useful for clinical practice.

Index Terms—Active contour model, cardiac MRI, cine MRI, iterative thresholding, left ventricle (LV) segmentation.

I. INTRODUCTION

CARDIAC disease is the leading cause of death in the USA and the developed world. The quantification of myocardial mass and systolic function is routinely performed in the clinical setting to diagnose a variety of cardiac pathologies. MRI, computed tomography (CT), ultrasound, X-ray, and single photon emission computed tomography (SPECT) can all be used to quantify cardiac function. However, MRI has several advantages including the lack of ionizing radiation exposure, the lack of nephrotoxic contrast injection, and the lack of geometric assumptions during volume measurements. Cardiac phase-resolved cine MRI is typically used to assess cardiac mechanical function. The left ventricle (LV) is segmented to estimate stroke volume, ejection fraction, and myocardial mass. Currently, manual tracing by an expert reader is the standard clinical practice. However, this task is labor-intensive and subject to inter- and intraobserver variability, due to inaccuracies in tracing complex myocardial structures such as papillary and trabecular muscles (PTMs).

Many algorithms have been introduced to reduce observer variation and improve time efficiency, as summarized in Section II. In this paper, an automatic LV segmentation algorithm for cardiac cine MRI images using iterative thresholding and an active contour model with adaptation (ITHACA) is presented. To segment the endocardium, the coil sensitivity of the magnitude image is corrected and a seed region-growing scheme is applied, where the threshold is determined iteratively by detecting the effusion into surrounding structures. To detect the epicardial contour and segment the myocardium (Myoc), a circular map (Cmap) is generated by polar mapping, and edge information is extracted on the Cmap and filtered using the endocardial segmentation. After defining an external force and constraints with information obtained from the endocardium segmentation, the active contour model (ACM) is applied to find the epicardial contour. We measured the blood volume and the myocardial volume of the LV using our ITHACA segmentation algorithm and compared this to manual tracing and the commercially available MASS analysis software (General Electric) in 38 subjects [2], [17].

II. RELATED WORKS

Many cardiac LV segmentation methods have been studied to calculate blood volume, myocardial volume, and ejection fraction using MRI. These methods can be categorized as follows: traditional segmentation, graph-based segmentation, active shape model (ASM), and level-set algorithms.

Traditional segmentation algorithms use thresholding, region-growing, edge-detection, and clustering [4]–[11]. Since these algorithms alone require significant user-interaction to segment LV, they have been combined with other segmentation techniques in hybrid schemes to minimize user-intervention. These algorithms work for mid-ventricular slices of LV, but

H.-Y. Lee was with the Department of Radiology, Weill Medical College of Cornell University, New York, NY 10022 USA. He is now with Kumoh National Institute of Technology, Gumi 730-701, Korea (e-mail: haeyeoun.lee@kumoh.ac.kr).

N. C. F. Codella is with the Department of Physiology, Biophysics, and Systems Biology, Weill Medical College of Cornell University, New York, NY 10022 USA (e-mail: noel.codella@gmail.com).

M. D. Cham and J. W. Weinsaft are with the Department of Radiology, Weill Medical College of Cornell University, New York, NY 10022 USA (e-mail: mac9166@med.cornell.edu; jww2001@med.cornell.edu).

*Y. Wang is with the Department of Radiology, Weill Medical College of Cornell University, New York, NY 10022, USA (e-mail: yiwang@med.cornell.edu).

Color versions of one or more of the figures in this paper are available online at http://ieeexplore.ieee.org.

Digital Object Identifier 10.1109/TBME.2009.2014545

have problems in basal and apical slices. Also, they are unable to segment the detailed structure of PTMs.

Graph-based segmentation algorithms create a graph with an assigned cost in each pixel or node and then find a minimum cost path using graph-searching algorithms such as iterative-programming or the A* algorithm [12]–[14]. These methods are unable to accurately segment complex cardiac structures such as PTMs, and have difficulties in the basal and apical slices.

ACMs segment objects through energy minimization of internal forces such as rigidity and elasticity, and external forces such as edges [15]–[17]. Contour initiation is critical to the success of ACM segmentation, as the algorithm is susceptible to local minima. In addition, ACMs have difficulty with low contrast images. ASMs, which are based on ACMs, segment objects using a shape model that is based on prior knowledge. The knowledge is represented by hand-annotated segmentation from a training dataset. Active appearance models (AAMs) are extensions of ASM that consider texture variation of objects with the shape of objects [3], [18]. Using a manual training dataset, the model is generated through principal component analysis, and the model is deformed according to the statistical variation of the dataset. ASM and AAM are limited in regard to the variation of the training dataset. Also, they impose high computational costs for iterative procedures. Moreover, ACM, ASM, and AAM have limitations in extracting the details of PTMs.

Level-set segmentation is a recent and well-established method to segment objects in noisy data [19]–[22]. However, it has difficulty in determining the stopping term, requires strong initialization of segmenting objects, and can get stuck in local minimum and high computational costs. Some algorithms use prior models to solve these problems, but the dependency on prior models results in loss of segmenting details and cardiac abnormalities.

In summary, much research has been performed in LV segmentation. Each algorithm has tradeoffs among time complexity, inter- or intraoperator variation, and accuracy in clinical practice. These algorithms have not segmented PTMs in detail.

III. AUTOMATIC LV SEGMENTATION

Our automatic LV segmentation algorithm consists of two parts: 1) a soft endocardial contour extraction by iterative thresholding, and 2) an epicardial contour extraction by active contour modeling.

A. Endocardial Contour Extraction by Iterative Thresholding

A soft endocardial contour segmentation algorithm was used [1], consisting of the following five steps.
1) Estimate the initial seed point.
2) Measure the mean and standard deviation of blood signal.
3) Compensate for coil sensitivity.
4) Estimate the myocardial (Myoc) signal intensity.
5) Segment the LV and measure the blood volume.

1) Step 1: Initial Seed Point Estimation: To identify a seed point within the LV cavity, a circular Hough transform is performed on the subtraction magnitude of images from phases 1 and 10 (roughly corresponding to diastole and systole, re-

spectively) of an initial mid-ventricular slice, selected by the user [3], [12], [14], [23]. A seed propagation technique is applied for remaining slices and phases, where the seed point for the current slice or phase image is determined by examining an 11×11 pixel window, whose center is the center of gravity of the segmented LV region in the previous image. The energy of each pixel in the window is calculated based on the distance from the center of the window and the intensity difference from the mean of LV region in the previous image

$$E(p) = \sqrt{\left(\frac{2\sigma_{\mathrm{prev}}}{w-1} \, |p_{\mathrm{CoG}} - p| \right)^2 + (I_{\mathrm{new}}(p) - \mu_{\mathrm{prev}})^2} \quad (1)$$

where p is the evaluated pixel position, $I_{\mathrm{new}}(p)$ is the intensity of the evaluated pixel, p_{CoG} is the center-of-gravity of LV region in the previous image, $w = 11$ is the window width in number of voxels, and σ_{prev} and μ_{prev} is the mean and standard deviation of LV region in the previous image. The first term of the equation penalizes pixels that are far away from the current seed point, and the second term penalizes pixels that deviate from the current blood intensity mean. The pixel with the lowest energy is chosen as the seed point.

2) Step 2: Mean and Standard Deviation of Blood Signal Estimation: Edge-based region-growing scheme is performed from the initial seed point to find an exact LV region that is nearly full-blood. The mean and standard deviation ($\mathrm{LV}_{\mathrm{mean}}$ and $\mathrm{LV}_{\mathrm{std}}$) of this exact LV region is calculated, and the voxels visited in this step are considered as full-blood in all subsequent calculations.

3) Step 3: Coil-Sensitivity Compensation: Images from MR scanner have distortions depending on coil location that can affect segmentation and volume calculations. To compensate coil sensitivity across the area of the LV, the intensity variation across the pool of full-blood voxels is modeled by a planar surface, which is determined by fitting the plane to the voxels of step 2 using least squares to attain the minimum residual.

4) Step 4: Myoc Signal Intensity Estimation: In order to estimate the mean signal intensity, $\mathrm{Myoc}_{\mathrm{mean}}$, of Myoc, successive lower-bound threshold-based region-growing scheme is run for an iteratively decreasing threshold, using the same seed as in step 2. Eventually, region growth breaks through the Myoc, "effusing" into surrounding structures (epicardial fat or fluids, right ventricle, muscle, liver, etc.), causing a sudden increase in the apparent segmented volume, which can be characterized by a discontinuity in a ratio of consecutive volume growth. The discontinuity of volume growth during decreasing region-growing threshold is used to measure the threshold at which region-growth has penetrated the Myoc. The threshold just before region-growth effuses into surrounding structures has been previously shown [1] to occur at approximately 1 standard deviation away from the mean signal intensity, $\mathrm{Myoc}_{\mathrm{mean}}$, of the Myoc, and is henceforth referred to as such.

5) Step 5: LV Segmentation and Volume Measurement: To segment the LV region, region growing is performed again for the last time within the image that slice or phase image using an absolute threshold of $\mathrm{Myoc}_{\mathrm{mean}} + n \times \mathrm{LV}_{\mathrm{std}}$, where $n = 2$. Accounting for Gaussian noise, the assignments ensure
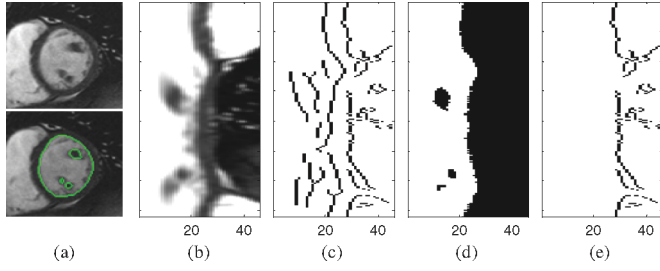
Fig. 1. (a) Input image and segmented LV by iterative thresholding. (b) Input image in polar coordinate. (c) Edge information by Canny detector. (d) LV in polar coordinate. (e) Filtered edge information.

at least 99.4% of full-blood and full-myocardium voxels will be weighted correctly. The total blood volume of the segmented LV is determined by the summation of pixels as follows:

$$V = \sum_x h(x)w(x) \qquad (2)$$

where V is volume and $h(x)$ is the histogram of the LV. $w(x)$ is the weighting function associated with blood voxels of intensity x and is used for calculating partial voxel effects. When $w(x) = 1.0$, the blood volume of the LV is calculated without partial voxel effects. Fig. 1(a) depicts the segmented LV cavity region by iterative thresholding. Since the absolute threshold $\text{Myoc}_{\text{mean}} + n \times \text{LV}_{\text{std}}$ is larger than the intensity of the PTM area, the presented algorithm excludes the PTM areas.

B. Epicardial Contour Extraction by ACM

For epicardial contour extraction, a modified application-specific ACM algorithm is developed. ACMs, also called snakes [24], [25], can be formulated as

$$E_{\text{snake}} = \int_0^1 \{E_{\text{internal}}C(s) + E_{\text{external}}C(s)\}ds \qquad (3)$$

where $C(s)$ is a list of contour points $(x(s), y(s))$, E_{internal} is an internal energy caused by bending contours, and E_{external} is the attraction of image features such as edges. The points in the contour iteratively approach the boundary or edge of an object through the minimization of the snake energy. The internal energy function is defined as

$$E_{\text{internal}} = \alpha(s)\left|\frac{dC}{ds}\right|^2 + \beta(s)\left|\frac{dC^2}{ds^2}\right|^2 \qquad (4)$$

where $\alpha(s)$ is a measure of the elasticity of the ACM and $\beta(s)$ is a measure of the stiffness of the ACM. The external energy function is defined by calculating the image $(f(x,y))$ gradients as

$$E_{\text{external}} = |\nabla f(x,y)|^2. \qquad (5)$$

A critical weakness of ACM is that it is susceptible to local minima; therefore, the initial contour should be defined near the searching objects. If the initial contour is located far from objects, it is difficult to define the external force and hence it does not converge to the desired segmentation. In this application, the problem is simplified, the intensity constraint is applied, and the external force is generated using prior knowledge even where

it is not clear what the direction of the force should be. These modifications for the epicardial contour extraction are explained in following five steps.

1) Generate a circular map through polar mapping about the endocardial center of mass.
2) Extract edge information and filter out the edge from the endocardium.
3) Define the external force and constraint for the epicardial contour.
4) Apply the epicardial ACM initialized at the endocardial contour.
5) Update the epicardial contour and transform the coordinates.

1) Step 1 (Circular Map Generation): Since the LV has roughly a circular shape, we generate a circular map (Cmap) by polar mapping, where the center of the polar mapping is the center-of-mass from the endocardial region in Section III-A. Through this mapping, (x, y) Cartesian image coordinates are converted to (radius r, radian θ) polar coordinates. The maximum radius is selected to cover all potential cardiac short-axis surface areas [see Fig. 1(a) and (b)].

2) Step 2 (Edge Information Extraction and Filtering): In the Cmap, edge information is extracted by applying the Canny edge extractor [26], where the sensitivity threshold and sigma in this study were set to 0.3 and 1.0, respectively. Since the endocardial region is segmented from iterative thresholding, edge information that comes from the endocardial region is filtered out [see Fig. 1(c)–(e)].

3) Step 3 (Modified External Force and Movement Constraint Definition): In standard ACMs, the external force is only well defined near the targeted objects typically using the gradient vector force (GVF), and the external force far from the targeted objects is difficult to define [24], [25]. Fig. 2(b) shows the external force defined by gradients, where gradient values in the red polygon are approximately zero. If a contour is seeded in those areas, there will be no sufficient external force to move the contour. In our LV segmentation applications, the contour is initialized at the endocardial border of LV as determined in Section III-A. For extracting the epicardial border, the initialized contour should move iteratively in the direction of increasing radius r. This prior knowledge can be used to condition the external force for effectively moving the contour in the following manner. After gradient calculation, gradients less than a predefined threshold are set to the closest values (along increasing radius) that are greater than the threshold. The threshold used in this study was 0.03 [see Fig. 2(c)].

The information on myocardial intensity, estimated from the iterative thresholding in Section III-A, is used to further constrain the contour movement. Let $\text{Myoc}_{\text{max}} = \text{Myoc}_{\text{mean}} + 2.0 \times \text{LV}_{\text{std}}$ and $\text{Myoc}_{\text{min}} = \text{Myoc}_{\text{mean}} \times 0.4$. Regions of signal intensity over Myoc_{max} or below Myoc_{min} (see Fig. 3) that are larger than 240 pixels are used as a constraint to block the movement of the contour. In MRI, since the intensity variation of myocardium can be substantial, we do not use $\text{Myoc}_{\text{mean}} - 2 \times \text{LV}_{\text{std}}$ as Myoc_{min}, but rather $\text{Myoc}_{\text{mean}} \times 0.4$ to accommodate these large variations. Small regions that are part of myocardium may still fall outside $[\text{Myoc}_{\text{min}}, \text{Myoc}_{\text{max}}]$, and
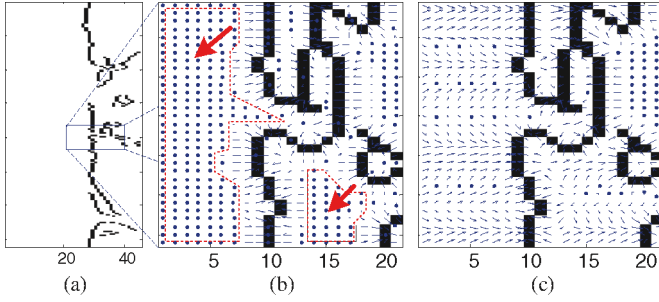
Fig. 2. (a) Edge information and clip location in blue rectangle. (b) Gradients without modification. (c) Gradients after modification.
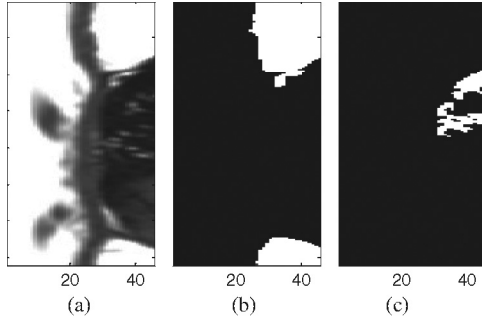

Fig. 3. (a) Input image in polar coordinate. (b) Region whose value is over $\text{Myoc}_{\max}$. (c) Region whose value is below $\text{Myoc}_{\min}$.

the minimal region size of 240 pixels is used to prevent these small regions of the myocardium from being excluded from the segmentation. The size of 240 pixels is determined experimentally, and is quite large in comparison to the expected number of myocardial pixels to fall outside the $\text{Myoc}_{\min}/\text{Myoc}_{\max}$ intensity range. Therefore, the performance of the algorithm is not sensitive to the value of this parameter.

4) Step 4 (Active Contour Model Segmentation): The ACM guided by the modified external force, and the movement constraint in step 3, is then applied for LV segmentation. The initial contour is set at the LV endocardial border determined from iterative thresholding in Section III-A. The elasticity α and stiffness β parameters of the internal energy in this study are set as 5.0 and 2.0, respectively. These parameters are experimentally determined. Since the lateral wall of myocardium locally looks like line on circular map, the internal energy is set to be higher than the external energy. While iteratively minimizing the energy, the contour is limited to only move in the radial direction r and stops if it meets the movement constraint. The average difference between contour points before and after each iteration is calculated and iteration is stopped if the average difference is below 0.01 pixels, which means that the internal and external energy is minimized. Fig. 4 shows the results after ACM segmentation. Fig. 4(a) and (b) represents a slice near to the basal slice, where the total iteration of ACM is 54 times. Fig. 4(c) and (d) represents a slice near to the apical slice, where the total iteration of ACM is 174 times. The blue line represents the initial contour that is the endocardial border. The green line represents the epicardial contour extracted by the ACM segmentation. The arrows in blue locate the points that stop moving by the con-

straint. Fig. 4(a) and (b) shows how the ACM stops because of the myocardial intensity constraint (blue arrows). Fig. 4(c) and (d) shows how the ACM stops where the edges are not defined or extracted (red arrow).

5) Step 5 (Epicardial Contour Updating and Coordinate Transform): Since the epicardial contour from ACM can have zigzag patterns, a low-pass filter is applied to make it smooth. Then, the epicardial contour is transformed in image domain by a simple inverse calculation of polar mapping in step 1.

IV. EXPERIMENTS AND RESULTS

A. Test Dataset

This retrospective analysis of existing patient data was approved by our Institutional Review Board (IRB) and performed in compliance with the Health Insurance Portability and Accountability Act. No informed consent was required. Data were acquired from cardiac MRI examinations previously performed on 38 patients (15 males, mean age: 52.4 years ±15.1 standard deviation). The most common clinical indications for referral of cardiac MRI were assessment of presence or pattern of myocardial scar. Cine steady-state free-precession (SSFP) scans were performed using a GE Signa 1.5 T scanner, imaging parameters TR 3.3–4.5 ms, TE 1.1–2.0 ms, flip angle 55–60, matrix size $192 \times 192 - 256 \times 256$, image dimensions 256×256, receiver bandwidth 125 kHz, field of view (FOV) 290–400×240 –360, slice thickness and slice gap 6–8 mm and 2–4 mm, respectively (total 10 mm). The LV in each patient was imaged in six to ten slices, 20–28 cardiac phases.

A total of 339 images from 38 patients were segmented by our ITHACA segmentation, with results compared to both manual tracing and the commercial MASS software [2], [3]. Manual tracing was performed by an experienced physician with PTMs excluded from the blood volume. PTMs were defined as myocardium protruding >1.5 mm from the circumferential contour of the LV cavity, with equivalent signal intensity to the adjacent LV wall.

B. Blood Volume and Myocardial Volume

Endocardial and myocardial volumes at diastole were measured using our ITHACA segmentation algorithm and the MASS software and compared with manual tracing. Calculated volumes are presented without partial volume interpolation as in the reference clinical manual tracing and MASS software, though our algorithm is capable of calculating partial volume using LV and Myoc intensity statistics. The difference between epicardial volume and endocardial volume is the myocardial volume, which, when multiplied by the known myocardial density of 1.05 g/mL, gives the myocardial mass. Linear regression and Bland–Altman analysis were performed to assess correlation between manual tracing, our ITHACA segmentation algorithm, and the MASS software.

Blood volume from manual tracing, our ITHACA segmentation, and the MASS software were 144.5 mL ±50.0 (average $\pm$ standard deviation), 141.6 mL ±48.7, and 164.5 mL ±55.1, respectively. Myocardial mass from manual tracing, our ITHACA
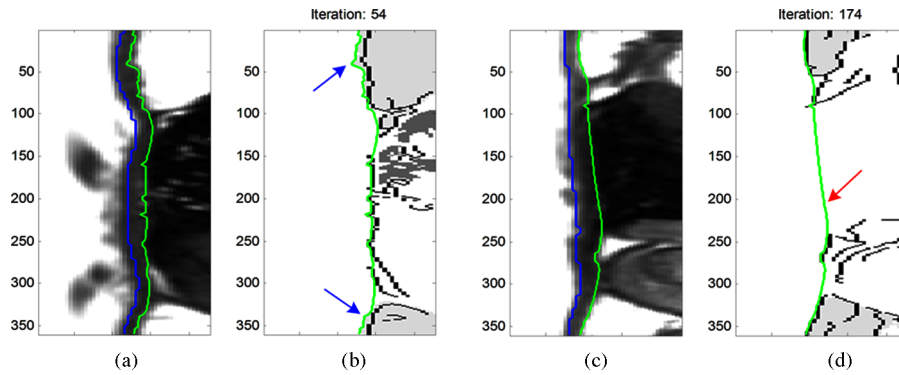
Fig. 4.   (a) Endocardial contour in blue and epicardial contour in green. (b) Edge information with constraint and epicardial contour by ACM whose total iteration was 54 times. (c) Endocardial contour in blue and epicardial contour in green. (d) Edge information with constraint and epicardial contour by ACM whose total iteration was 174 times. In (c) and (d), the edge information pointed by red arrow is intentionally removed to depict how the ITHACA algorithm works with low contrast cases.
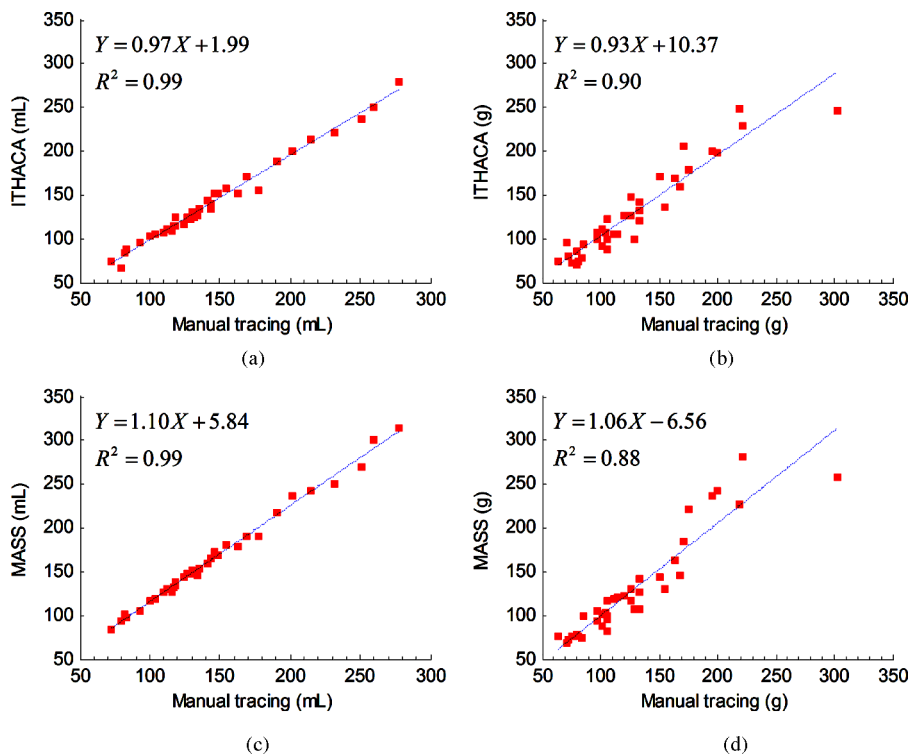

Fig. 5.   (a) and (b) Blood volume and myocardial mass in diastolic phase from our ITHACA segmentation. (c) and (d) MASS software correlate with that from manual tracing.

segmentation, and the MASS software were 128.1 ± 50.9 g, 128.9 ± 49.0 g, and 129.1 ± 57.5 g, respectively. Comparisons of these measurements are summarized in Table I and Figs. 5 and 6. Blood volumes measured from our ITHACA algorithm and the MASS software correlated highly with that from manual tracing ($R^2 = 0.99$), and myocardial mass measurements were fairly correlative ($R^2 = 0.90$ and 0.88 for ITHACA and MASS, respectively). The Bland–Altman analysis (Fig. 6) indicated that the myocardial mass measurements agreed with each other very well, the blood volume measured from the ITHACA algorithm agreed well with that from manual tracing, but the blood volume measured from the MASS software was substantially higher than that from manual tracing due to the inclusion of PTMs in the LV blood by the MASS software.

TABLE I
VOLUME COMPARISON BETWEEN OUR SEGMENTATION AND MASS SOFTWARE AGAINST MANUAL CONTOURING IN 38 PATIENTS

	Manual tracing – ITHACA algorithm			Manual tracing – MASS software		
	Absolute	Relative	Corr.	Absolute	Relative	Corr.
Endocardial volume	2.9±6.2 (mL)	1.8±4.5 (%)	R²=0.99	-20.0±6.9 (mL)	-14.3±3.3 (%)	R²=0.99
Epicardial volume	2.0±13.0 (mL)	0.5±4.1 (%)	R²=0.98	-21.0±20.8 (mL)	-7.7±5.6 (%)	R²=0.96
Myocardial mass	-0.9±16.5 (g)	-1.5±11.9 (%)	R²=0.90	-1.0±20.2 (g)	0.0±12.3 (%)	R²=0.88

The performances of the ITHACA algorithm and the MASS software were summarized in Table II. An example case of segmentation using all three methods is illustrated in Fig. 7.
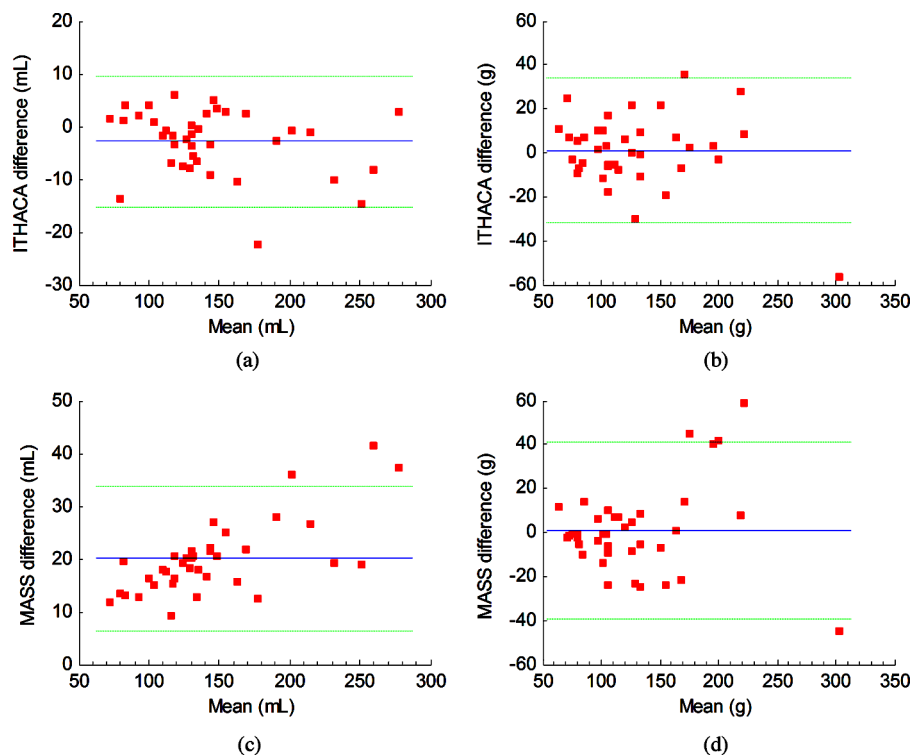
Fig. 6.   (a) and (b) Bland–Altman plots of blood volume and myocardial mass from our segmentation and (c)–(d) MASS software compared with that from manual tracing.

TABLE II
USER-INTERVENTION COMPARISON BETWEEN OUR ITHACA SEGMENTATION AND MASS SOFTWARE IN 38 PATIENTS

		ITHACA algorithm	MASS software
Endocardial contour	Basal slices	16/339, 4.7 % (16/38, 42.1 %)	17/339, 5.0 % (17/38, 44.7 %)
	Other slices	0/339, 0 % (0/38, 0 %)	36/339, 10.6 % (28/38, 73.6 %)
Epicardial contour	Additional slices	5/339, 1.5 % (5/38, 13.1 %)	175/339, 51.6 % (38/38, 100.0 %)

(Unumbers based on patient are in parenthesis)

Either of these two automated software was judged to fail when generating a contour that deviated from the ventricle border by more than 10% in area as visually estimated by the operator, as illustrated in Fig. 7. When this occurred, the operator performed manual correction on the contour. Both ITHACA and MASS software required manual intervention, 4.7% and 5.0%, respectively, at some basal-most slices (almost half of the patient cases), because of the lack of myocardial enclosure. For generating endocardial contour, the MASS software required manual intervention in most apical slices, and the ITHACA algorithm eliminated this problem. For generating epicardial contour, the MASS software required manual intervention for 51.6% slices, and the ITHACA algorithm reduced the need for manual intervention to 1.5% slices (near-complete automation).

The ITHACA algorithm allowed automatic segmentation over all cardiac phases. An example of LV volumes versus cardiac phase is illustrated in Fig. 8. The myocardial mass, derived from the difference between epicardial volume and endocardial

volume, is fairly constant over cardiac phases. The maximal and minimal endocardial volumes of 73.4 mL and 27.1 mL, respectively, can be easily identified to calculate an ejection fraction of 63.1%. Values obtained using manual tracing were similar: 72.2 mL, 24.7 mL, and 65.8%, respectively. MASS measured the ejection fraction at 69.6%.

V. DISCUSSION

Our experimental data indicate that the proposed ITHACA segmentation algorithm is highly accurate and robust in segmenting the LV mass and blood volume. This ITHACA algorithm provides a substantial improvement over the commercial MASS software that requires manual intervention in almost every patient. While automated segmentation at the cardiac basal slice remains a concern, the ITHACA algorithm succeeds in eliminating the need for manual intervention at other slices (mostly apical slices) when segmenting the endocardial border, and almost eliminates manual intervention when segmenting the epicardial border. Comparison with the clinical standard of manual tracing suggests that the ITHACA algorithm can be a valuable clinical tool for the rapid quantification of LV stroke volume, ejection fraction, and myocardial mass.

The ITHACA algorithm starts to extract the endocardial border using the geometrical assumption that bright blood is surrounded by dimmer myocardium. This simple assumption does not require specific LV shape knowledge, and it is valid for all slices except for the basal-most slice where the LV outflow tract disrupts the closure of myocardium. By seeding at the LV blood,
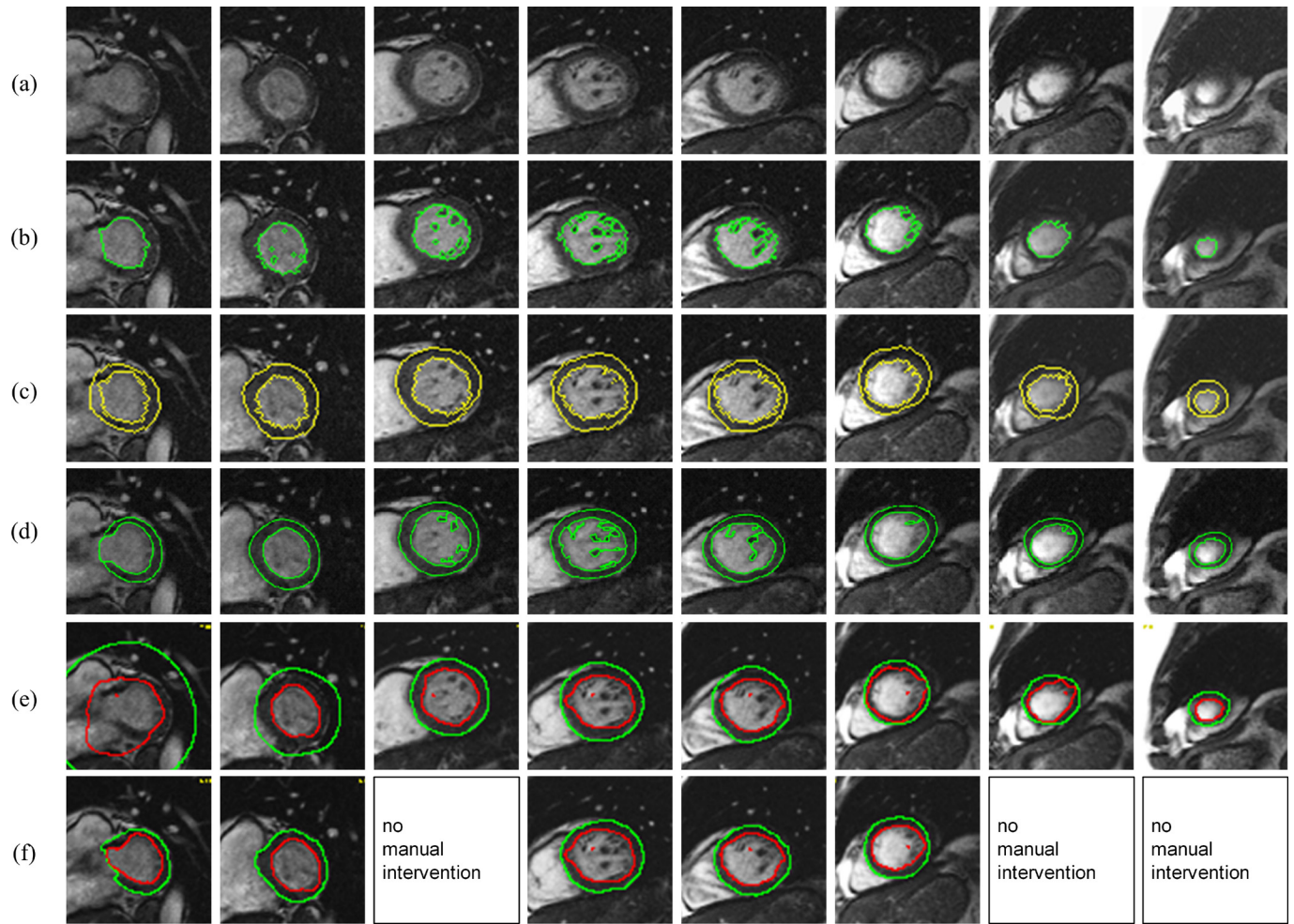
Fig. 7. Segmentation results in patient 29. (a) Intensity images. (b) LV cavity. (c) Myocs from our ITHACA algorithm. (d) LV cavity and Myocs by manual tracing, LV cavity and Myocs from MASS (e) before, and (f) after manual intervention.
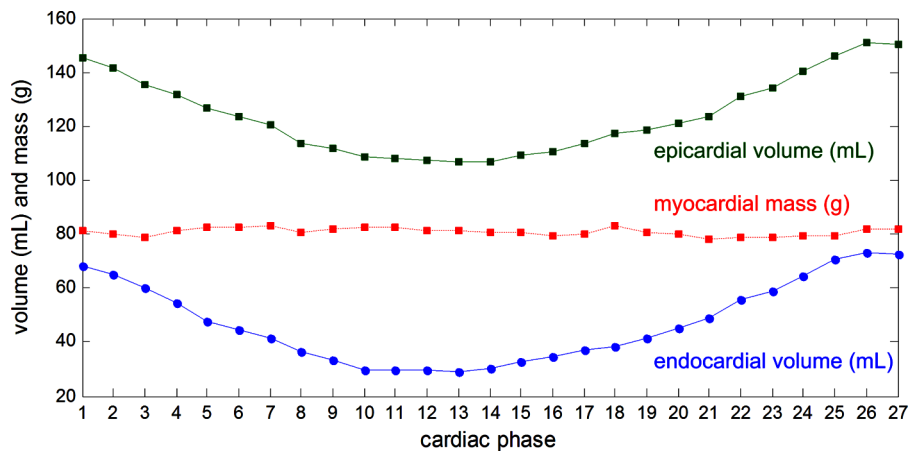

Fig. 8. Endocardial volume, epicardial volume, and myocardial mass versus cardiac phase change in a patient using the ITHACA algorithm.

the blood and myocardial signal intensity profile can be estimated from region growth through iterative thresholding. The critical threshold is identified by the abrupt increase in region growth. This iterative thresholding approach in guiding region growth turns out to be very robust in automatically extracting LV blood.

The ITHACA algorithm extracts the outer epicardial border using the ACM, which is adapted to or guided by the endocardial border and signal intensity profile already determined from the first part of iterative thresholding. The external force is conditioned to drive the contour from the endocardial border toward the epicardial border, and the search for epicardial border

is further efficiently localized by blocking areas with intensity above or below myocardial signal. This adaptation makes the ACM converge rapidly onto the epicardial border through a few iterations. Our experimental data indicate that this ACM with adaptation is quite robust in automatically extracting the epicardial border, enabling estimation of the LV myocardial mass.

The ITHACA algorithm did not eliminate the need for manual intervention when extracting the epicardial border in 1.5% of slices, where the signal intensity difference between myocardium and surrounding tissues (lung or liver) was almost zero. Experienced clinicians can draw a separation between myocardium and its surrounding based upon their training. This *a priori* knowledge of the epicardial border shape may be incorporated in the conditioning of the ACM. Similarly, *a priori* knowledge of the outflow tract at the basal-most slice for the endocardial border may be incorporated to condition the region growth and completely eliminate manual intervention. On the other hand, the ITHACA algorithm is probably more accurate at segmenting complex borders than manual tracing, causing a slight disagreement between manual tracing and our ITHACA algorithm. This kind of segmentation error was under 10% and was not corrected by user-intervention.

While manual tracing is not a perfect reference, the inter- and intraoperator variability in contour generation can be quite small for experienced readers. Our two clinicians independently and repeatedly after 2 weeks traced a subset of ten patients. The corresponding intraoperator variations were $-1.35\% \pm 1.85$ (-1.81 mL ± 2.36) for endocardial volume and $4.53\% \pm 6.59$ (4.83 g ± 7.44) for myocardial mass. Interoperator variations were $-2.41\% \pm 2.12$ (-3.23 mL ± 3.3) for endocardial volume and $6.0\% \pm 8.39$ (6.88 mL ± 9.95) for myocardial mass. Accordingly, manual tracing by an experienced clinician can be used as the reference standard. However, there is a concern with current full-voxel-based volume calculations from manual tracing used in clinical practice. All voxels with mixtures of blood and myocardium do require proper partial volume calculation by scaling to blood and myocardium signal. Under the current imaging protocol of fairly thick slices (10 mm including gap), this partial volume effect may be substantial. The ejection fraction calculation may not be affected substantially if both systole and diastole volumes are affected by a similar ratio. A gold standard for blood volume measurement is required to assess these partial volume effects.

Currently, the ITHACA segmentation algorithm was implemented in MATLAB, and it took about 3 s to process a slice, and 30 s to process a cardiac phase (eight to ten slices). If the algorithm is implemented and optimized in C or C++, each phase would be processed within several seconds. Although the ACM is used, its execution time is short, because the prior knowledge of the endocardial border and myocardial signal estimated from the first part of the ITHACA algorithm is used to guide the energy minimization.

The ITHACA algorithm is based on the fact that myocardium and blood on cardiac cine MRI have different intensities. As long as there is sufficient tissue contrast, the ITHACA algorithm may be applied with little modification on cardiac image data acquired from various imaging parameters, pulse sequences, and other imaging modalities like CT and US.

VI. CONCLUSION

We have developed an automated algorithm for segmenting the LV from short-axis cine cardiac MRI images. Iterative thresholding is used first to identify the endocardial border and estimate the blood and myocardium signal profile, which are then used to guide the ACM for rapidly extracting the epicardial border. We term this algorithm as ITHACA. Our experimental data from 38 patients showed that the ITHACA algorithm provided substantial improvement over the commercial MASS software in LV segmentation and provided segmentation results similar to the current clinical standard of manual tracing. Although the ITHACA algorithm performed better than the MASS software in aspects of manual intervention and accuracy, manual intervention is still required at basal slices. The ITHACA algorithm was tested on cine SSFP images on 1.5 T. Future work will consider automation at basal slices and evaluation on data acquired with different sequences, field strength, and modalities.

REFERENCES

[1] N. Codella, J. W. Weinsaft, M. D. Cham, M. Janik, M. R. Prince, and Y. Wang, "Left ventricle: Automated segmentation by using myocardial effusion threshold reduction and intravoxel computation at MR imaging," *Radiology*, vol. 248, no. 3, pp. 1004–1012, Sep. 2008.

[2] R. J. van der Geest, E. Jansen, V. G. M. Buller, and J. H. C. Reiber, "Automated detection of left ventricular epi- and endocardial contours in short-axis MR images," in *Proc. IEEE Comput. Cardiol.*, Sep. 1994, pp. 33–36.

[3] R. J. Van Der Geest, B. P. Lelieveldt, E. Angelie, M. Danilouchkine, C. Swingen, M. Sonka, and J. H. Reiber, "Evaluation of a new method for automated detection of left ventricular boundaries in time series of magnetic resonance images using an active appearance motion model," *J. Cardiovasc. Magn. Reson.*, vol. 6, no. 3, pp. 609–617, 2004.

[4] L. P. Clarke, R. P. Velthuizen, M. A. Camacho, J. J. Heine, M. Vaidyanathan, L. O. Hall, R. W. Thatcher, and M. L. Silbiger, "MRI segmentation: Methods and applications," *Magn. Reson. Imag.*, vol. 13, no. 3, pp. 343–368, 1995.

[5] J.S. Suri, "Computer vision pattern recognition and image processing in left ventricle segmentation: The last 50 years," *Pattern Anal. Appl.*, vol. 3, pp. 209–242, 2000.

[6] A. E. O. Boudraa, M. Arzi, J. Sau, J. Champier, S. Hadj-Moussa, J.-E. Besson, D. Sappey-Marinier, R. Itti, and J.-J. Mallet, "Automated detection of the left ventricular region in gated nuclear cardiac imaging," *IEEE Trans. Biomed. Eng.*, vol. 43, no. 4, pp. 430–437, Apr. 1996.

[7] A. E. O. Boudraa, "Automated detection of the left ventricular region in magnetic resonance images by Fuzzy C-Means model," *Int. J. Card. Imag.*, vol. 13, no. 4, pp. 347–355, 1997.

[8] G. D. Waiter, F. I. McKiddie, T. W. Redpath, S. I. Semple, and R. J. Trent, "Determination of normal regional left ventricular function from cine-MR images using a semi-automated edge detection method," *Magn. Reson. Imag.*, vol. 17, pp. 99–107, 1999.

[9] A. S. Pednekar, R. Muthupillai, V. V. Lenge, I. A. Kakadiaris, and S. D. Flamm, "Automatic identification of the left ventricle in cardiac cine-MR images: Dual-contrast cluster analysis and scout-geometry approaches," *J. Magn. Reson. Imag.*, vol. 23, no. 5, pp. 641–651, 2006.

[10] M. Lynch, O. Ghita, and P. F. Whelan, "Left-ventricle myocardium segmentation using a coupled level-set with a priori knowledge," *Comput. Med. Imag. Graph.*, vol. 30, pp. 255–262, 2006.

[11] Z. Zhou, J. You, P. A. Heng, and D. Xia, "Cardiac MR image segmentation and left ventricle surface reconstruction based on level set method," *Stud. Health Technol.*, vol. 111, pp. 629–632, 2005.

[12] R. J. Van Der Geest, V. G. M. Buller, E. Jansen, H. J. Lamb, L. H. B. Baur, E. E. Van Der Wall, A. de Roos, and J. H. C. Reider, "Comparison between manual and semiautomated analysis of left ventricle volume parameters from short-axis MR images," *J. Comput. Assisted Tomogr.*, vol. 21, no. 5, pp. 756–765, 1997.

[13] R. J. van Geuns, T. Baks, E. H. Gronenschild, J. P. Aben, P. A. Wielopolski, F. Cademartiri, and P. J. de Feyter, "Automatic quantitative left ventricular analysis of cine MR images by using three-dimensional information for contour detection," *Radiology*, vol. 240, no. 1, pp. 215–221, 2006.

[14] A. Pednekar, U. Kurkure, R. Muthupillari, S. Flamm, and I. A. Kakadiaris, "Automated left ventricle segmentation in Cardiac MRI," *IEEE Trans. Biomed. Eng.*, vol. 53, no. 7, pp. 1425–1428, Jul. 2006.

[15] M. F. Santarelli, V. Positano, C. Michelassi, M. Lombardi, and L. Landini, "Automated cardiac MR image segmentation: Theory and measurement evaluation," *Med. Eng. Phys.*, vol. 25, no. 2, pp. 149–159, 2003.

[16] M. R. Kaus, J. von Berg, J. Weese, W. Niessen, and V. Pekar, "Automated segmentation of the left ventricle in cardiac MRI," *Med. Image Anal.*, vol. 8, no. 3, pp. 245–254, 2004.

[17] M.-P. Jolly, "Automatic segmentation of the left ventricle in cardiac MR and CT Images," *Int. J. Comput. Vis.*, vol. 70, no. 2, pp. 151–163, 2006.

[18] Q. Chen, Z. M. Zhou, M. Tang, P. A. Heng, and D. S. Xia, "Shape statistics variational approach for the outer contour segmentation of left ventricle MR Images," *IEEE Trans. Inf. Technol. Biomed.*, vol. 10, no. 3, pp. 588–597, Jul. 2006.

[19] W. J. Niessen, B. M. T. H. Romeny, and M. A. Viergever, "Geodesic deformable models for medical image analysis," *IEEE Trans. Med. Imag.*, vol. 17, no. 4, pp. 634–641, Aug. 1998.

[20] N. Paragios, "A level set approach for shape-driven segmentation and tracking of the left ventricle," *IEEE Trans. Med. Imag.*, vol. 22, no. 6, pp. 773–776, Jun. 2003.

[21] C. Corsi, C. Lamberti, R. Battani, A. Maggioni, G. Discenza, P. MacEneaney, V. Mor-Avi, R. M. Lang, and E. G. Caiani, "Computerized quantification of left ventricular volumes on cardiac magnetic resonance images by level set method," *Comput. Assisted Radiol. Surg.*, vol. 1268, pp. 1114–1119, 2004.

[22] M. Lynch, O. Ghita, and P. F. Whelan, "Automatic segmentation of the left ventricle cavity and myocardium in MRI data," *Comput. Biol. Med.*, vol. 36, no. 4, pp. 389–407, 2006.

[23] J. Illingworth and J. Kittler, "A survey of the Hough transform," *Comput. Vis., Graph., Image Process.*, vol. 44, no. 1, pp. 87–116, 1988.

[24] M. Kass, A. Witkin, and D. Terzopoulos, "Snakes: Active contour models," *Int. J. Comput. Vis.*, vol. 1, pp. 321–331, 1988.

[25] C. Xu and J. L. Prince, "Snakes, shapes, and gradient vector flow," *IEEE Trans. Image Process.*, vol. 7, no. 3, pp. 359–369, Mar. 1998.

[26] J. Canny, "A computational approach to edge detection," *IEEE Trans. Pattern Anal. Mach. Intell.*, vol. PAMI-8, no. 6, pp. 679–698, Nov. 1986.

Hae-Yeoun Lee received the M.S. and Ph.D. degrees in computer science from Korea Advanced Institute of Science and Technology (KAIST), Daejeon, Korea, in 1997 and 2006, respectively.

From 2001 to 2006, he was with Satrec initiative, Korea. From 2006 to 2007, he was a Postdoctoral Researcher at Weill Medical College, Cornell University, New York. He is currently a Professor at Kumoh National Institute of Technology, Gumi, Korea. His current research interests include medical image processing, remote sensing, digital watermarking, media forensics and digital right managements.

Noel C. F. Codella received the B.S. degree in computer science from Fu Foundation School of Engineering and Applied Science, Columbia University, Ithaca, NY, in 2004, and the M.Eng. degree in computer science from Cornell University in 2005. He is currently working toward the Ph.D. degree in the Department of Physiology, Biophysics, and Systems Biology, Weill Medical College, Cornell University, New York.

His current research interests include medical image processing, MR data-acquisition techniques, pulse sequence design, and projection self-navigator techniques.

Matthew D. Cham received the Graduate degree (with a double-major) from the University of Rochester, New York, and the M.D. degree (with distinction in research) from the School of Medicine and Dentistry, University of Rochester.

He completed his radiology residency at the University of Rochester—Strong Memorial Hospital. He was a Thoracic Radiology Research Fellow at Weill Cornell Medical College. He was a Cardiovascular MRI Fellow at the Imperial College School of Medicine—Royal Brompton Hospital, London. He is currently an Assistant Professor of Radiology at Weill Cornell Medical College, New York. He is board certified in diagnostic radiology. His research interests include noninvasive cardiovascular imaging, lung cancer imaging, and minimally invasive computed tomography (CT)-guided procedures.

Dr. Cham received the RSNA Roentgen Resident Research Award at the University of Rochester—Strong Memorial Hospital.

Jonathan W. Weinsaft received the medical degree from New York University, New York.

He completed his internal medicine residency and cardiology fellowships at Weill Medical College, Cornell University and Duke University. He is currently an Assistant Professor of medicine and radiology at New York Presbyterian Hospital, Cornell University Weill Medical Center, New York. His current research interests include the use of MRI for assessment of myocardial performance and infarct characterization.

Yi Wang received the B.S. degree in 1986 in nuclear physics from Fudan University, Shanghai, China, in 1986, and the Ph.D. degree in medical physics from University of Wisconsin, Madison, in 1994.

He is currently the Faculty Distinguished Professor of Radiology and Biomedical Medical Engineering, Cornell University, New York. His current research interests include rapid imaging techniques for cardiovascular MRI, navigator methodology for suppressing motion artifacts in cardiac MRI, segmentation methods for cardiac imaging, and magnetic nanoparticles for diagnosis and treatment.